INSTITUTE FOR HIGH ENERGY PHYSICS

IHEP 93-37
ОТФ

G. Jikia[1]

Z-boson Pair Production via Photon Fusion at High Energy Photon Linear Collider

Submitted to *Nucl. Phys.* B

[1]E-mail: jikia@mx.ihep.su

Protvino 1993

УДК 539.1.01

М-24

Abstract

G.V.Jikia. Z-bozon Pair Production via Photon Fusion at High Energy Photon Linear Collider: IHEP Preprint 93-37. - Protvino, 1993. - p. 31, refs.: 38.

The production of the Z-boson pairs via the fusion $\gamma\gamma \to ZZ$ of two polarized backscattered laser photons at an e^+e^- linear collider is considered. Complete one-loop SM calculation is done and explicit formulas for bosonic loop contributions to the helicity amplitudes are given. The results are used to study Higgs boson production for $m_H > 2m_Z$ at a Photon Linear Collider. It is shown that transversely polarized Z_TZ_T pair production would represent a severe irreducible background to the observation of the Higgs boson with $m_H > 350$ GeV if Z-boson polarization would not be detected. Total cross section of Z_TZ_T pair production is as large as hundreds of femtobarns at $\sqrt{s_{\gamma\gamma}} \geq 500$ GeV and does not decrease with energy. The anticipated photon-photon luminosity should be sufficient to detect hundreds of Z-boson pairs yearly. The reaction $\gamma\gamma \to ZZ$ may provide tests of anomalous triple and quartic gauge boson couplings.

Аннотация

Г.В.Джикия. Парное рождение Z бозонов в высокоэнергичных фотон-фотонных столкновениях и сигнал от Хиггсовского бозона: Препринт ИФВЭ 93-37. — Протвино, 1993. — 31 с., библиогр.: 38.

Проделано полное вычисление амплитуды реакции $\gamma\gamma \to ZZ$ в Стандартной Модели. Вклад W бозонной петли оказался значительным. Он приводит к большому сечению рождения пары поперечно поляризованных Z бозонов Z_TZ_T равному 200 фбн при $\sqrt{s_{\gamma\gamma}} = 500$ ГэВ для неполяризованных начальных фотонов. Парное образование Z_TZ_T будет приводить к большому неприводимому фону при наблюдении образования пары продольных Z бозонов Z_LZ_L. Таким образом, наблюдение сигнала от Хиггсовского бозона для $M_H \geq 500$ ГэВ на фотонном линейном коллайдере, если не разделять продольную и поперечную поляризации Z бозонов, представляется затруднительным.

1. Introduction

Higgs bosons search and/or electroweak symmetry breaking mechanism study will be major goals for the next generation of supercolliders [1]. Much has been written on the search for the Standard Model (SM) Higgs boson at hadron supercolliders (see, *e.g.*, Refs. [2] for recent reviews and further references). It is generally believed that a SM Higgs boson of a mass up to 1 TeV can be discovered at the SSC and LHC if the design luminosities are achieved. Next to the era of the hadron supercolliders lies the future generation of high energy e^+e^- linear colliders. The Next Linear Collider (NLC) is a generic name for a 500 GeV e^+e^- collider with a luminosity of order 10^{33} cm^{-2} s^{-1}. SM Higgs bosons up to 350 GeV in mass can be detected at the NLC [3]. However, it is very likely that the existence of the Higgs boson will have already been settled by hadron supercolliders before the NLC begins operations. Thus, one must carefully consider what the goals should be for an NLC intent on exploring Higgs physics. It was emphasized the NLC potential to settle definitely the question of the existence of an intermediate mass Higgs boson ($m_W < m_H < 2m_Z$) and , once the Higgs boson mass is known, to measure a number of key Higgs properties — its spin, electroweak quantum numbers and the Higgs couplings to weak bosons and heavy fermion pairs [4]. In addition, one may have the capability of running the NLC in a $\gamma\gamma$ collision mode via Compton backscattering of laser photons off the linear collider electrons [5–9]. The Higgs boson produced in such collisions would provide an accurate measurement of the $H\gamma\gamma$ coupling. This coupling is induced at the one-loop level and receives contributions from all virtual charged particles

whose masses are derived from the Higgs mechanism. Thus, the detection of Higgs bosons in the $\gamma\gamma$ collider mode at the NLC can provide fundamental information about the particle spectrum and mass generation mechanism of the theory. Moreover, at the SSC/LHC a rough determination of the Higgs boson $\gamma\gamma$ coupling (by detecting the rare $H \to \gamma\gamma$ decay mode) may only be possible for $90 < m_H < 130$ GeV [10]. (For recent experimental summaries see various SSC and LHC detector Letters of Intent and the SDC detector Technical Design Report [11–14].)

The background for the detection of $\gamma\gamma \to H \to X$ depends upon the choice of the final state X. For the SM Higgs boson with a mass below $2m_W$ the primary modes are $H \to b\bar{b}$ and $H \to ZZ^*, WW^*$ (where one virtual weak boson is produced off-shell). For this case careful study of the background from $\gamma\gamma \to b\bar{b}$ has been done, assuming the ability to achieve substantial polarization for the colliding photon beams [4, 7, 15]. The optimistic conclusion was reached [15] that the detection of the SM H should be possible for all Higgs masses up to the $\gamma\gamma$ kinematic limit (roughly $E_{\gamma\gamma}^{max} \simeq 0.8E_{e^+e^-}$). For the SM Higgs boson heavier than $2m_W$ the primary modes are $H \to ZZ, W^+W^-$ and $H \to t\bar{t}$. The conclusion of [15] is that detection of the H in the $t\bar{t}$ channel is not possible even for perfect polarization. Because of the large size of the $\gamma\gamma \to W^+W^-$ background a reasonable statistical significance can be achieved only in a narrow Higgs mass range near $2m_W$. As for ZZ mode the usual attitude is that since there is no tree-level $\gamma\gamma \to ZZ$ background, it will be advantageous to focus on the ZZ final state for $m_H > 2m_Z$, and when the ZZ final state can be cleanly isolated, the ability to detect the H in the ZZ decay mode will be entirely determined by the absolute event rate. The conclusion of [15] is that the ZZ mode can be used all the way out to 500 GeV, assuming the requirement of 5 signal events for detection.

The main irreducible background to detecting a Higgs boson in the ZZ decay mode in photon fusion reaction is the continuum production of Z boson pairs via the one-loop reaction $\gamma\gamma \to ZZ$. Although the process is of fourth order in coupling and one could naïvely expect its cross section to be negligible, the result of our calculation is that the transverse Z_TZ_T pair production cross section is as large as hundred of femtobarns. And if one does not separate longitudinal and transverse polarizations of the Z bosons the continuum production of Z boson pairs will prevent the detection of the Higgs boson signal in $\gamma\gamma$ collisions for $m_H \geq 350$ GeV.

There were also several other proposals why to study Z pair production in high energy photon-photon collisions. It was proposed to study the lon-

gitudinally polarized Z_LZ_L pair production to establish a signal from the heavy Higgs boson [16] and to probe strong final-state interaction corrections due to strongly-interacting Higgs sector [17]. The effects of a strongly interacting symmetry breaking sector in $\gamma\gamma \to Z_LZ_L$ reaction at TeV energies were analyzed in [18] by using Chiral Lagrangians. The existence of ultraheavy quanta with a mass generated by electroweak symmetry breaking can be probed in scattering of photon pairs into longitudinal Z pairs at energies large compared to m_W but small compared to the production threshold of the ultraheavy particles [19]. It was also suggested to study anomalous vector boson Higgs [20] and quartic vector boson couplings [21] in this reaction. All of these suggestions imply the deviations from the SM predictions for the longitudinal Z boson pair production cross sections at high invariant mass of the gauge boson pair. However, the weak vector boson t- and u-channel exchanges lead to a non decreasing with energy cross section for the loop-induced reaction $\gamma\gamma \to ZZ$ in analogy to the well known behaviour of the tree level process $\gamma\gamma \to W^+W^-$ [22]. Moreover, the SM cross sections for the transverse Z boson pair production are an order of magnitude larger than the signal from longitudinal Z boson pair production. So, careful treatment of the large irreducible background from the SM continuum Z boson pair production is needed to achieve any realistic estimate of the high energy $\gamma\gamma$ collisions potential to probe new physics. The cross section of the Z_TZ_T pair production being large and observable can be interesting by itself as an unambiguous nonlinear effect predicted by the SM as a nonabelian gauge theory.

Until recently only fermion loop contribution has been calculated for the reaction $gg \to ZZ$ [23, 24]. In Ref. [25] we presented some results of our first complete SM calculation of the helicity amplitudes for the reaction $\gamma\gamma \to ZZ$. In this paper we give the full details of the calculation. In Section 2, we will present the general formalism for the calculation of the $\gamma\gamma \to ZZ$ helicity amplitudes. In Section 3, we will give explicit analytic results for the bosonic loop contributions to the helicity amplitudes and their asymptotic expressions in the high energy limit. Section 4 will contain numerical results. Cross sections of the ZZ pair production in monochromatic polarized $\gamma\gamma$ collisions will be given in Section 4.1. Section 4.2 will contain cross sections of the ZZ pair production and the background to Higgs boson signal from transversely polarized Z_TZ_T pair production, calculated taking into account spectrum of the Compton backscattered polarized laser beams off polarized electron beams. ZZ pair production in photon fusion reactions at e^+e^- colliders

(Section 4.2) and at heavy-ion colliders (Section 4.3) will also be considered. Finally, in Section 5, conclusions will be done.

2. Definitions

We concentrate mainly on the most difficult boson loop contribution to the process

$$\gamma(p_1) + \gamma(p_2) \to Z(p_3) + Z(p_4). \tag{2.1}$$

To avoid the mixed photon-W-NG triple vertices and photon-Higgs-W-NG quartic vertices, containing non-physical Nambu-Goldstone scalars, we use the so-called nonlinear background gauge, which was used, *e.g.*, to calculate the two photon Higgs decay width [26]. Gauge fixing (GF) lagrangian and Faddeev-Popov (FP) ghost lagrangian parts in the background gauge contributing to the process under consideration are given by

$$\begin{aligned}
\mathcal{L}_{GF} &= -\left|\partial_\mu W^\mu - igs_W A_\mu W^\mu + (m_W + \frac{g}{2}H)w\right|^2 \\
&\quad -\frac{1}{2}\Big(\partial_\mu Z^\mu + (m_W + \frac{g}{2}H)\frac{z}{c_W}\Big)^2 - \frac{1}{2}(\partial_\mu A^\mu)^2 \quad , \qquad (2.2)\\
\mathcal{L}_{FP} &= -(\partial_\mu + igs_W A_\mu)\bar{c}^+(\partial^\mu - igs_W A^\mu - igc_W Z^\mu)c^+ \\
&\quad +m_W^2 \bar{c}^+ c^+ + gm_W H \bar{c}^+ c^+ \\
&\quad -(\partial_\mu - igs_W A_\mu)\bar{c}^-(\partial^\mu + igs_W A^\mu + igc_W Z^\mu)c^- \\
&\quad +m_W^2 \bar{c}^- c^- + gm_W H \bar{c}^- c^- \quad , \qquad (2.3)
\end{aligned}$$

where w, z are NG nonphysical partners of a W, Z bosons, $c^\pm$, $\bar{c}^\pm$ are FP ghost and antighost fields, $s_W = \sin\theta_W$, $c_W = \cos\theta_W$. The Feynman diagrams contributing to process (2.1) are shown in Fig. 1.

As it was done in the pioneering papers [27, 28], the $\gamma\gamma ZZ$ polarization tensor can be written in the form

$$\begin{aligned}
G^{\mu_1\mu_2\mu_3\mu_4} &= \sum_{i_1,i_2,i_3,i_4} A^{i_1 i_2 i_3 i_4}(1234) p_{i_1}^{\mu_1} p_{i_2}^{\mu_2} p_{i_3}^{\mu_3} p_{i_4}^{\mu_4} \\
&+ \sum_{i_3,i_4} B_1^{i_3 i_4}(1234) g^{\mu_1\mu_2} p_{i_3}^{\mu_3} p_{i_4}^{\mu_4} + \ldots + \sum_{i_1,i_2} B_6^{i_1 i_2}(1234) g^{\mu_3\mu_4} p_{i_1}^{\mu_1} p_{i_2}^{\mu_2} \qquad (2.4)\\
&+ C_1(1234) g^{\mu_1\mu_2} g^{\mu_3\mu_4} + C_2(1234) g^{\mu_1\mu_3} g^{\mu_2\mu_4} + C_3(1234) g^{\mu_1\mu_4} g^{\mu_2\mu_3}.
\end{aligned}$$

Here $i_{1,2} = 3, 4$, $i_{3,4} = 1, 2$. The restrictions on the summation of the indices $i_{1\ldots4}$ take into account the momenta conservation, transversality of the

polarization vectors and, in addition, maintain a symmetric appearance of $G^{\mu_1\mu_2\mu_3\mu_4}$. All momenta are taken to be on mass shell ($p_1^2 = p_2^2 = 0, \quad p_3^2 = p_4^2 = m_Z^2$). The electromagnetic gauge invariance tells us that the $\gamma\gamma ZZ$ polarization tensor is transversal to the photon momenta

$$p_1^{\mu_1} e_2^{\mu_2} e_3^{\mu_3} e_4^{\mu_4} G_{\mu_1\mu_2\mu_3\mu_4} = 0 = p_2^{\mu_2} e_1^{\mu_1} e_3^{\mu_3} e_4^{\mu_4} G_{\mu_1\mu_2\mu_3\mu_4}. \tag{2.5}$$

Relations among A, B and C coefficients in (2.4) following from Bose symmetry, gauge invariance (2.5) and Schouten identities were given in Ref. [25].

We define

$$\begin{aligned} s = (p_1 + p_2)^2, \quad t = (p_2 + p_3)^2, \quad u = (p_1 + p_3)^2, \\ s_4 = s - 4m_Z^2, \quad t_1 = t - m_Z^2, \quad u_1 = u - m_Z^2, \\ Y = tu - m_Z^4 = s \cdot p_{TZ}^2, \quad \beta = \sqrt{1 - 4m_Z^2/s}. \end{aligned} \tag{2.6}$$

All momenta are taken to be incoming.

3. The $\gamma\gamma \to ZZ$ helicity amplitudes

We use the reduction algorithm of Ref. [29] to express all A, B and C coefficients (2.4) in a canonical form in terms of the set of basic scalar loop integrals described in Ref. [30]. The algebraic calculations were carried out using symbolic manipulation program FORM [31].

Using the full polarization tensor (2.4) helicity amplitudes can be derived

$$\mathcal{M}_{\lambda_1\lambda_2\lambda_3\lambda_4} = e_1^{\mu_1}(\lambda_1) e_2^{\mu_2}(\lambda_2) e_3^{\mu_3 *}(\lambda_3) e_4^{\mu_4 *}(\lambda_4) G_{\mu_1\mu_2\mu_3\mu_4}(p_1, p_2, p_3, p_4), \tag{3.1}$$

where λ_i denotes the polarization of particle i. The momenta and polarization vectors for different helicities in the c.m.s. of the initial photons are given by

$$\begin{aligned} p_1 = E(1; 0, 0, 1), \quad p_2 = E(1; 0, 0, -1), \\ p_3 = -E(1; \beta \sin\theta_Z, 0, \beta \cos\theta_Z), \quad p_4 = -E(1; -\beta \sin\theta_Z, 0, -\beta \cos\theta_Z); \end{aligned} \tag{3.2}$$

$$\begin{aligned} e_1^+ = e_2^- = \tfrac{1}{\sqrt{2}}(0; -1, -i, 0), \quad e_1^- = e_2^+ = \tfrac{1}{\sqrt{2}}(0; +1, -i, 0), \\ e_3^{+*} = e_4^{-*} = \tfrac{1}{\sqrt{2}}(0; -\cos\theta_Z, +i, +\sin\theta_Z), \\ e_3^{-*} = e_4^{+*} = \tfrac{1}{\sqrt{2}}(0; +\cos\theta_Z, +i, -\sin\theta_Z), \\ e_3^0 = \tfrac{E}{m_Z}(\beta; \sin\theta_Z, 0, \cos\theta_Z), \quad e_4^0 = \tfrac{E}{m_Z}(\beta; -\sin\theta_Z, 0, -\cos\theta_Z). \end{aligned} \tag{3.3}$$

Here $e^{\pm}$ is γ or Z boson polarization vector with helicity ± 1 and e^0 is the longitudinal polarization vector of the Z boson.

The helicity amplitudes are related by parity (or CP-parity for fermion loop contribution) and Bose symmetry

$$\begin{aligned}\mathcal{M}_{\lambda_1\lambda_2\lambda_3\lambda_4}(s,t,u,\beta) &= \mathcal{M}_{-\lambda_1-\lambda_2-\lambda_3-\lambda_4}(s,t,u,\beta),\\ \mathcal{M}_{\lambda_1\lambda_2\lambda_3\lambda_4}(s,t,u,\beta) &= \mathcal{M}_{\lambda_2\lambda_1\lambda_4\lambda_3}(s,t,u,\beta).\end{aligned} \tag{3.4}$$

Using the composition of a rotation by 180^0 about the y-axis and parity transformation, the remaining twelve amplitudes can be expressed through eight independent helicity amplitudes

$$\begin{aligned}\mathcal{M}_{++--}(s,t,u,\beta) &= \mathcal{M}_{++++}(s,t,u,-\beta),\\ \mathcal{M}_{++-0}(s,t,u,\beta) &= -\mathcal{M}_{+++0}(s,t,u,-\beta),\\ \mathcal{M}_{+--+}(s,t,u,\beta) &= \mathcal{M}_{+-+-}(s,t,u,-\beta),\\ \mathcal{M}_{+--0}(s,t,u,\beta) &= -\mathcal{M}_{+-+0}(s,t,u,-\beta).\end{aligned} \tag{3.5}$$

We write the bosonic loop contribution to helicity amplitudes as a sum of three terms

$$\mathcal{M}_{\lambda_1\lambda_2\lambda_3\lambda_4} = A_{\lambda_1\lambda_2\lambda_3\lambda_4} + S_{\lambda_1\lambda_2\lambda_3\lambda_4} + \mathcal{M}^H_{\lambda_1\lambda_2\lambda_3\lambda_4}, \tag{3.6}$$

where $S_{\lambda_1\lambda_2\lambda_3\lambda_4}$ is subamplitude containing singular factors of $1/Y \sim 1/p_{TZ}^2$ and $\mathcal{M}^H_{\lambda_1\lambda_2\lambda_3\lambda_4}$ is the Higgs pole contribution.

Extracting an overall factor

$$\frac{e^2g^2}{(4\pi)^2}, \qquad \text{where } g = \frac{e}{s_W}, \tag{3.7}$$

in the definition of the helicity amplitudes $\mathcal{M}_{\lambda_1\lambda_2\lambda_3\lambda_4}$, we find the nonzero subamplitudes $A_{\lambda_1\lambda_2\lambda_3\lambda_4}$, $S_{\lambda_1\lambda_2\lambda_3\lambda_4}$ and $\mathcal{M}^H_{\lambda_1\lambda_2\lambda_3\lambda_4}$:

$$\begin{aligned}&A_{+++-}(s,t,u,\beta) =\\ &\Big\{-C(t)2x_Zm_Z^2\Big[1+\frac{m_Z^2}{s_4t_1}(s-2m_Z^2)+\frac{t_1}{s}\Big(1-\frac{Y}{c_W^2ss_4}\Big)\Big]\\ &+D(s,t)2M_1^4\Big(c_W^2-\frac{m_Z^2}{s_4}\Big)-B(t)x_{WZ}m_Z^2\Big(2\frac{t}{s}-1\Big)\frac{Y}{s_4t_1^2} \quad + \quad (t\leftrightarrow u)\Big\}\\ &+D(t,u)x_Zm_Z^2\Big(\frac{Y}{s}+2m_W^2\Big)\Big(1-\frac{Y}{c_W^2ss_4}\Big)\\ &+C(s)4x_Zm_Z^2-C_0(s)2x_Zm_Z^2\Big(1+2\frac{m_Z^2}{s_4}\Big)-\frac{x_{WZ}Y}{t_1u_1}\Big(1+2\frac{m_Z^2}{s_4}\Big);\end{aligned} \tag{3.8}$$

$$
\begin{aligned}
&A_{++++}(s,t,u,\beta) = \\
&\Big\{D(s,t)\Big[2M_1^4\frac{m_Z^2}{s_4}+4c_W^2s^2+2(m_Z^2-4m_W^2-8c_W^2m_W^2)s-6c_W^2M_2^4 \\
&+\beta\Big(16\frac{m_Z^6}{s_4}+4c_W^2s^2+2(m_Z^2-8c_W^2m_W^2)s+4m_Z^4\Big)\Big] \\
&+C(t)\Big[\frac{t_1}{s}\Big(16c_W^2s+6m_Z^2-24m_W^2-24c_W^2m_W^2 \\
&-\frac{x_{WZ}Y}{ss_4}(s-2m_Z^2)\Big)+2\frac{M_1^4}{s_4t_1}(s-2m_Z^2) \\
&+\beta\Big\{t_1\Big(\frac{1}{s_4}(6m_Z^2+8m_W^2-24c_W^2m_W^2-\frac{x_{WZ}Y}{s})+16c_W^2\Big)+2M_1^4\frac{s}{s_4t_1}\Big\}\Big] \\
&+B(t)\frac{x_{WZ}}{2s_4}\left((1+\beta)s-2m_Z^2\right)\left(2\frac{m_Z^4}{t_1^2}-2\frac{t}{s}-1\right) \quad + \quad (t\leftrightarrow u)\Big\} \qquad (3.9)\\
&+D(t,u)\Big[\frac{Y}{2}\Big(\frac{x_{WZ}Y}{s^2s_4}(s-2m_Z^2)+\frac{x_Zm_Z^2}{s_4}-\frac{1}{s}(5m_Z^2-20m_W^2-36c_W^2m_W^2) \\
&-16c_W^2\Big)+4c_W^2s(s-2m_Z^2-4m_W^2)-6c_W^2M_2^4 \\
&+\beta\Big\{\frac{Y}{2s_4}\Big(\frac{x_{WZ}Y}{s}-16c_W^2s-4m_Z^2+48m_W^2+48c_W^2m_W^2\Big)+4c_W^2s(s-4m_W^2)\Big\}\Big] \\
&+C_0(s)\frac{4}{s_4}(M_1^4+2\beta m_Z^2s)+\frac{x_{WZ}}{s_4t_1u_1}\left(m_Z^2(2Y-ss_4)+\beta sY\right);
\end{aligned}
$$

$$
\begin{aligned}
&A_{++00}(s,t,u,\beta) = \\
&\Big\{-D(s,t)\Big[4\frac{M_1^4m_Z^2}{s_4}-4m_W^2s+m_Z^4-12m_W^2m_Z^2+44m_W^4\Big] \\
&+C(t)\Big[\frac{t_1}{s}\Big(4\frac{x_{WZ}m_Z^2Y}{ss_4}-\frac{m_Z^2}{c_W^2}-4m_Z^2+20m_W^2\Big)-8\frac{M_1^4m_Z^2}{s_4t_1}\Big] \\
&+B(t)\frac{x_{WZ}m_Z^2}{s_4}\Big[4\frac{t}{s}+2-4\frac{m_Z^4}{t_1^2}\Big] \quad + \quad (t\leftrightarrow u)\Big\} \qquad (3.10)\\
&+D(t,u)\Big[Y\Big\{-\frac{x_{WZ}}{s_4}\Big(2\frac{m_Z^2Y}{s^2}+m_W^2\Big)+\frac{m_Z^2}{2c_W^2s}(1-2c_W^2)(1+8c_W^2-12c_W^4)\Big\} \\
&+4m_W^2s+m_Z^4+4m_W^2m_Z^2-20m_W^4\Big]-C_0(s)4\Big[s+2\frac{M_1^4}{s_4}\Big]-4\frac{x_{WZ}m_Z^2Y}{s_4t_1u_1};
\end{aligned}
$$

$$
\begin{aligned}
&A_{+++0}(s,t,u,\beta)/\Delta = \\
&\Big\{D(s,t)\Big[1+\frac{x_Z m_Z^2}{s_4}+\beta\frac{s}{s_4}\Big](Y+t^2-m_Z^4) \\
&+C(t)\Big[(t-u)\frac{t_1}{s}\Big(\frac{x_{WZ}Y}{ss_4}-2\Big)-2\frac{x_Z m_Z^2}{s_4}\Big(m_Z^2\frac{s}{t_1}+s-2m_Z^2\Big) \\
&+\beta\Big\{(t-u)\frac{t_1}{s_4}\Big(\frac{x_{WZ}}{s}\Big(\frac{Y}{s}+2m_W^2\Big)-2\Big)-2\frac{x_Z m_Z^2}{s_4}\Big(m_Z^2\frac{s}{t_1}+s-2m_Z^2\Big)\Big\}\Big] \\
&+B(t)(1+\beta)\frac{x_{WZ}Y}{s_4}\Big[\frac{m_Z^2}{t_1}\Big(\frac{1}{t_1}-\frac{2}{s}\Big)-\frac{2}{s}\Big] \quad - \quad (t\leftrightarrow u)\Big\} \qquad (3.11) \\
&+D(t,u)(t-u)Y\Big[\frac{1}{4s}(5-4c_W^2+12c_W^4)-\frac{x_{WZ}}{4s_4}\Big(2\frac{Y}{s^2}+c_W^2\Big) \\
&+\frac{\beta}{2}\Big\{\frac{1}{s_4}(1-2c_W^2)(1+6c_W^2)-\frac{x_{WZ}}{s}\Big(\frac{Y}{ss_4}-c_W^2\Big)\Big\}\Big] \\
&-C_0(s)2(t-u)\Big[1+\frac{x_Z m_Z^2}{s_4}+\beta\frac{s}{s_4}\Big]-(1+\beta)\frac{x_{WZ}(t-u)Y}{s_4 t_1 u_1};
\end{aligned}
$$

$$
\begin{aligned}
&A_{+-++}(s,t,u,\beta) = \\
&\Big\{D(s,t)\Big[\frac{2}{s_4}(2m_Z^2Y-8m_W^2t_1^2+M_1^4m_Z^2)-6c_W^2M_2^4\Big] \\
&+C(t)\frac{2}{s_4}\Big[x_Z m_Z^2(s-2m_Z^2)\Big(\frac{u_1}{s}-\frac{m_Z^2}{t_1}\Big)-16m_W^2t_1\Big] \\
&+B(t)\frac{x_{WZ}m_Z^2}{s_4t_1^2}\Big[Y+2m_Z^2t\Big] \quad + \quad (t\leftrightarrow u)\Big\} \qquad (3.12) \\
&+D(t,u)\Big[\frac{Y}{2}\Big(\frac{1}{s_4}(32m_W^2+x_Z m_Z^2)+\frac{x_Z m_Z^2}{s}\Big)-6c_W^2M_2^4\Big] \\
&+C(s)\Big[2\frac{x_{WZ}m_Z^4}{s_4}-6y_Z m_Z^2\Big]-C_0(s)32\frac{m_W^2 s}{s_4}-\frac{x_{WZ}Y}{t_1u_1}\Big(1+2\frac{m_Z^2}{s_4}\Big);
\end{aligned}
$$

$$
\begin{aligned}
&A_{+-+-}(s,t,u,\beta) = \\
&\Big\{D(s,t)\Big[\frac{2}{s_4}\Big(2(m_Z^2+4m_W^2)t^2+4m_Z^2(m_Z^2-4m_W^2)t \\
&+m_Z^2(m_Z^4+12m_W^2m_Z^2-12m_W^4)\Big)+2c_W^2(4t^2+2s^2+5m_Z^4) \\
&+2(m_Z^2-4m_W^2)(2t+s)+8c_W^2m_W^2(2s-m_Z^2+3m_W^2) \\
&+2\beta\frac{s}{s_4}\Big\{4c_W^2m_W^2(t-u)-(s-2m_Z^2)(2c_W^2s+x_Zm_Z^2)\Big\}\Big] \\
&+C(t)\Big[x_Zm_Z^2\Big(2\frac{m_Z^2}{t_1}\Big(1+2\frac{m_Z^2}{s_4}\Big)-\frac{t_1}{s}\Big)+16c_W^2t_1 \\
&+\frac{1}{s_4}\Big((m_Z^2+28m_W^2+12c_W^2m_W^2)t+3m_Z^4-44m_W^2m_Z^2+36m_W^4\Big) \\
&-\beta\frac{2}{s_4}\Big\{(x_Zm_Z^2+4c_W^2s)(t-u)-4c_W^2s^2-x_Zm_Z^2(s-2m_Z^2)+M_1^4\frac{s}{t_1}\Big\}\Big] \\
&+B(t)x_{WZ}\Big[2\frac{m_Z^4}{s_4t_1}+\frac{m_Z^4}{t_1^2}\Big(1+2\frac{m_Z^2}{s_4}\Big)-\frac{1}{2}+\frac{m_Z^2}{s_4} \\
&-\beta\Big\{2\frac{m_Z^4}{s_4t_1}+m_Z^4\frac{s}{s_4t_1^2}+2\frac{t}{s_4}-\frac{1}{2}\Big\}\Big] \quad + \quad (t\leftrightarrow u,\beta\to-\beta)\Big\} \qquad (3.13) \\
&+D(t,u)\Big[-x_Zm_Z^2\frac{t_1^2}{2s}+4c_W^2(2t^2+2st+s^2) \\
&+\frac{1}{2s_4}(m_Z^2+28m_W^2+12c_W^2m_W^2)(t+m_Z^2)^2-8c_W^2(m_Z^2-2m_W^2)s \\
&+2c_W^2(5m_Z^4-4m_W^2m_Z^2+12m_W^4)-4\beta c_W^2s(t-u)\Big\{1+\frac{2}{s_4}(m_Z^2+2m_W^2)\Big\}\Big] \\
&+C(s)\Big[4x_{WZ}\Big(m_W^2-\frac{Y}{s_4}+2\frac{m_Z^4}{s_4}\Big)+\frac{s}{c_W^2}(3-12c_W^2+52c_W^4) \\
&+\beta x_{WZ}(t-u)\Big\{5+\frac{4}{s_4}(t+5m_Z^2+m_W^2)+\frac{4}{s_4^2}(t^2+2m_Z^2t+4m_Z^4)\Big\}\Big] \\
&+C_0(s)16c_W^2s\Big(1+2\frac{m_Z^2}{s_4}\Big)+B(s)x_{WZ}\Big(1+2\frac{m_Z^2}{s_4}\Big)\Big[3+4\beta\frac{t-u}{s_4}\Big] \\
&+\frac{x_{WZ}}{s_4t_1u_1}\Big(Y(s-2m_Z^2)+\beta m_Z^2s(t-u)\Big);
\end{aligned}
$$

$$
\begin{aligned}
&A_{+-+0}(s,t,u,\beta)/\Delta = \\
&\Big\{D(s,t)\Big[\frac{t-u}{s_4}\Big(4c_W^2(t^2+m_Z^2t+2m_Z^4)+\frac{t^2}{c_W^2}-(t-2m_Z^2)(2t+m_Z^2) \\
&+(1+8c_W^2)s_4t-12c_W^2m_W^2i\Big)-2\frac{t_1}{s_4}\Big(x_{WZ}t^2-(t+m_Z^2)(16c_W^2t+x_Zm_Z^2)\Big) \\
&+\beta\Big\{\frac{Y}{s_4}(s+8c_W^2s+40c_W^2m_W^2) \\
&-\frac{1}{s_4}\Big(24c_W^2m_W^2t_1^2+s(t^2-8c_W^2t(2t+m_Z^2)+m_Z^4)\Big)\Big\}\Big] \\
&+C(t)\Big[(t-u)\Big\{\Big(\frac{2}{ss_4}\Big(4c_W^2(t+3m_Z^2)-\frac{t}{c_W^2}+4t-3m_Z^2\Big)t_1-24c_W^2m_W^2u_1\Big) \\
&+2\frac{M_1^4}{s_4t_1}+2\frac{t-4m_W^2}{s_4}\Big\}+4\frac{t_1^2}{ss_4}\Big(x_{WZ}t-16c_W^2(t+m_Z^2)\Big) \\
&+\frac{\beta}{s_4}\Big\{2Y+2(1-16c_W^2)(t+m_Z^2)t_1+8c_W^2(m_Z^2-3m_W^2)(t-u)-2M_1^4\frac{s}{t_1}\Big\}\Big] \\
&+B(t)\frac{x_{WZ}}{s_4}\Big[m_Z^2(t-u)\frac{t}{t_1^2}+t+m_Z^2-\beta\Big\{m_Z^4\frac{s}{t_1^2}+m_Z^2\frac{s}{t_1}+t+m_Z^2\Big\}\Big] \\
&\quad -\quad (t\leftrightarrow u,\beta\to-\beta)\Big\} \qquad (3.14) \\
&-D(t,u)Y\Big[\frac{t-u}{s}\Big(1+\frac{1}{s_4}(8c_W^2s+x_Zm_Z^2)\Big)-\beta\Big\{1+8\frac{c_W^2}{s_4}(s+8m_W^2)\Big\}\Big] \\
&-C(s)\Big[2(t-u)\Big(2\frac{x_{WZ}m_Z^2}{s_4}+\frac{(1-2c_W^2)^2}{c_W^2}\Big)+\beta\Big\{2x_{WZ}m_Z^2\Big(1+4\frac{m_Z^2}{s_4}\Big)+\frac{y_Zs}{c_W^2}\Big\}\Big] \\
&+C_0(s)\Big[(t-u)\Big(6+4c_W^2-\frac{1}{c_W^2}-4m_Z^2\frac{y_Z}{c_W^2s_4}\Big) \\
&-2\beta\Big\{x_Zm_Z^2\Big(1+4\frac{m_Z^2}{s_4}\Big)+(1-8c_W^2)s\Big\}\Big] \\
&-B(s)x_{WZ}\frac{t-u+\beta s}{s_4}+\frac{x_{WZ}Y(t-u-\beta s)}{s_4t_1u_1};
\end{aligned}
$$

$$
\begin{aligned}
&A_{+-00}(s,t,u,\beta) = \\
&\Big\{D(s,t)\Big[\frac{4}{s_4}\Big(m_Z^2(2t^2+4m_Z^2t+m_Z^4)+4m_W^2(2t^2-4m_Z^2t+3m_Z^4)\\
&-12m_W^4m_Z^2\Big)+2t^2+4m_Z^2t-4m_W^2(s-3m_Z^2)+m_Z^4-44m_W^4\Big]\\
&+C(t)\Big[4t_1\Big(1+16\frac{m_W^2}{s_4}\Big)+8\frac{M_1^4}{s_4}\Big(\frac{t_1}{s}+\frac{m_Z^2}{t_1}+1\Big)\Big]\\
&+B(t)2\frac{x_{WZ}m_Z^2}{s_4t_1^2}(t^2+m_Z^4) \quad + \quad (t\leftrightarrow u)\Big\} \qquad (3.15)\\
&-D(t,u)\Big[2Y\Big(1+\frac{2}{s_4}\Big(\frac{M_1^4}{s}+8m_W^2\Big)\Big)+4m_W^2(s-m_Z^2)-m_Z^4+20m_W^4\Big]\\
&-C(s)\Big[4\frac{x_{WZ}m_Z^4}{s_4}+4s+\frac{m_Z^2}{c_W^2}-12m_Z^2+44m_W^2\Big]\\
&+C_0(s)4s\Big[1+16\frac{m_W^2}{s_4}\Big]+4\frac{x_{WZ}m_Z^2Y}{s_4t_1u_1};
\end{aligned}
$$

$$
\begin{aligned}
&S_{+-+-}(s,t,u,\beta) = x_{WZ}\Big\{\frac{1}{Y}\Big[\Big(Q(s,t,u)t+Q(s,u,t)u\Big)\Big(2m_W^2-\frac{m_Z^4}{s_4}\Big)\\
&+\frac{\beta}{s_4}\Big(t(2m_W^2(t-u)+st)Q(s,t,u)-u(2m_W^2(u-t)+su)Q(s,u,t)\Big)\Big]\\
&+\frac{1}{2Y^2}\Big(tQ_2(s,t,u)+uQ_2(s,u,t)\Big)\Big(1+\beta\frac{t-u}{s_4}\Big)\Big\}; \qquad (3.16)\\
&S_{+-+0}(s,t,u,\beta)/\Delta = \\
&\frac{x_{WZ}}{2s_4Y}\Big(t^2Q(s,t,u)+u^2Q(s,u,t)\Big)(t-u+\beta s); \qquad (3.17)\\
&S_{+-++}(s,t,u,\beta) = -\frac{R_{+-++}}{s_4Y}\Big(tQ(s,t,u)+uQ(s,u,t)\Big); \qquad (3.18)\\
&S_{+-00}(s,t,u,\beta) = -\frac{R_{+-00}}{s_4Y}\Big(tQ(s,t,u)+uQ(s,u,t)\Big); \qquad (3.19)\\
&S_{+++-}(s,t,u,\beta) = \frac{x_Zm_Z^2}{Y}\Big(tQ(s,t,u)+uQ(s,u,t)\Big); \qquad (3.20)
\end{aligned}
$$

$$
\mathcal{M}^H_{++++} = \frac{(8sm_Z^2-12m_W^2m_Z^2-2m_Z^2m_H^2)C_0(s)-m_H^2/c_W^2-6m_Z^2}{s-m_H^2+im_H\Gamma_H}; \qquad (3.21)
$$

$$\mathcal{M}^H_{++00} = \mathcal{M}^H_{++++}\frac{s-2m_Z^2}{2m_Z^2}. \tag{3.22}$$

Here the following notations were used:

$$\begin{aligned}
&R_{+-00} = 2s^2 + \frac{m_Z^2 s}{2c_W^2} - 14m_Z^2 s + 22m_W^2 s + 16m_Z^4 - 64m_W^2 m_Z^2,\\
&R_{+-++} = 3m_Z^2 s - 12m_W^2 s - 12c_W^2 m_W^2 s - \frac{m_Z^4}{c_W^2} - 8m_Z^4 + 36m_W^2 m_Z^2 + 48m_W^4;\\
&M_1^4 = m_Z^4 - 4m_W^2 m_Z^2 + 12m_W^4, \quad M_2^4 = m_Z^4 - 4m_W^2 m_Z^2 - 4m_W^4;\\
&\Delta = \sqrt{\frac{sm_Z^2}{2Y}}, \quad x_{WZ} = \frac{M_1^4}{m_W^2 m_Z^2}, \quad x_Z = \frac{M_1^4}{m_Z^4}, \quad y_Z = \frac{M_2^4}{m_Z^4}.
\end{aligned} \tag{3.23}$$

The B, C and D functions are the basic two-, three- and four-point integrals described in Appendix A. Auxiliary functions Q and Q_2, which are always associated with a pole in Y, are also defined in the Appendix A.

Various checks were carried out to make sure that the resulting helicity amplitudes are correct. All A, B and C coefficients in the decomposition of the polarization tensor (2.4) were calculated. Then cancellation of divergences, the requirements of Bose symmetry and gauge invariance (2.5) were explicitly checked. Also, subamplitudes containing factors of $1/Y \sim 1/p_{TZ}^2$ (3.16-3.20) were shown to be finite as $p_{TZ} \to 0$ (see Appendix A). In practice to avoid numerical instabilities we made a small p_{TZ} cut. And finally, we compared numerically the values of the imaginary parts of all the helicity amplitudes given by (3.6) with the values obtained via unitarity relations from the tree level amplitudes evaluated in unitarity gauge. We obtained that both values coincided to an accuracy of ten digits over a wide range of kinematical variables.

In the high energy limit with u held finite and large

$$s \gg -u \gg m_W^2, m_Z^2, \tag{3.24}$$

which corresponds to Z production at small angle

$$\theta_Z \sim (-u/s)^{1/2} \tag{3.25}$$

only two helicity conserving amplitudes survive, which are imaginary and proportional to s

$$\mathcal{M}_{++++} = \mathcal{M}_{+-+-} = -16\pi i\frac{s}{u}c_W^2 \log(-u/m_W^2). \tag{3.26}$$

In the same limit the leading fermion loop contributions to helicity amplitudes grow only as logarithm squared

$$\mathcal{M}^f_{++++} = \mathcal{M}^f_{+-+-} = -4(v_f^2 + a_f^2)\log^2(-s/u), \tag{3.27}$$

where

$$v_f = (t_{3L}(f)/2 - Q_f s_W^2)/c_W, \quad a_f = t_{3L}(f)/2c_W.$$

This difference can be traced back to the effect of the u-channel vector particle exchange, which gives rising amplitudes and nondecreasing corresponding total cross section in the limit $s \to \infty$ and finite u (see, *e.g.*, Ref. [32] for a thorough review and references therein). The imaginary parts of the helicity amplitudes at $\theta_Z = 0$ in the high energy limit can be easily calculated via unitarity relations given the helicity amplitudes of the reaction $\gamma\gamma \to W^+W^-$ [22]

$$\Im m\mathcal{M}_{++++}(\theta_Z = 0) = \Im m\mathcal{M}_{+-+-}(\theta_Z = 0) = 8\pi s c_W^2/m_W^2. \tag{3.28}$$

The corresponding real parts can be shown via dispersion relations to have no contributions proportional to s, because the growing contribution from s-channel discontinuity is completely cancelled by the t-channel discontinuity contribution.

In the high energy limit (3.24) the cross section of the transverse Z boson pair production is dominated by the contribution from production at small angles (3.26) and is given by

$$\sigma_{++++} = \sigma_{+-+-} = \frac{16\pi\alpha^4}{-u_{min}}\frac{c_W^4}{s_W^4}\left[\log^2(-u_{min}/m_W^2) + 2\log(-u_{min}/m_W^2) + 2\right]. \tag{3.29}$$

As for longitudinal Z pair production, the corresponding helicity amplitudes have no contributions proportional to s and the leading amplitude in the high energy limit and for large Higgs boson mass s, $m_H^2 \gg m_W^2, m_Z^2$ is proportional to m_H^2/m_W^2. It comes from Higgs pole contribution (3.22) and is given by

$$\mathcal{M}_{++00} = -\frac{m_H^2}{2m_W^2}\frac{s}{s - m_H^2}. \tag{3.30}$$

This expression coincides with the result obtained in [16] using the equivalence theorem approximation.

For fermion loop contributions to helicity amplitudes we agree with expressions given in [24] except the overall signs. We define the fermion helicity

amplitudes using the same momenta and polarization vectors (3.2), (3.3) and including the factor -1 for fermion loop. With these assignments all our helicity amplitudes except $\mathcal{M}_{+++0}$, $\mathcal{M}_{+-+0}$ differ from the corresponding expressions in [24] by a factor -1. Amplitudes $\mathcal{M}_{+++0}$, $\mathcal{M}_{+-+0}$ coincide with the corresponding amplitudes of ref. [24] if we define the quantity $\sqrt{-2m_Z^2/sY}$ in ref. [24] to be equal to $i\sqrt{2m_Z^2/sY}$.

4. Numerical Results

4.1. Polarized cross sections for ZZ pair production in monochromatic $\gamma\gamma$ collisions

We first present different contributions to the polarized cross sections for ZZ pair production in monochromatic $\gamma\gamma$ collisions. We consider here the extreme cases of $\lambda_{\gamma 1}\lambda_{\gamma 2} = \pm 1$, *i.e.* full circular polarization for the incoming photons. The cross section is given by

$$\frac{d\hat{\sigma}_{\lambda_1,\lambda_2,\lambda_3,\lambda_4}(\hat{s})}{d\cos\theta_Z} = \frac{\alpha^2\alpha_W^2}{2\hat{s}}\left|\mathcal{M}_{\lambda_1\lambda_2\lambda_3\lambda_4}\right|^2\frac{\beta}{16\pi}, \tag{4.1}$$

where for identical particles the integration over $\cos\theta_Z$ should be done from 0 to 1. The parameters $\alpha_W = \alpha/s_W^2$, $\alpha = 1/128$, $m_Z = 91.173$ GeV, $m_W = 80.22$ GeV and $s_W^2 = 1 - m_W^2/m_Z^2$ have been used throughout the paper.

In Fig. 2 we present total cross sections as well as separate contributions from W-boson loop, all fermion loop and top quark loop for different polarizations of the initial photons and outgoing Z-bosons. If not stated otherwise, top quark mass was assumed to be 120 GeV. Completely polarized initial photons are considered. As is shown in Fig. 2a, Higgs boson signal is clearly seen in Z_LZ_L pair production for equal initial photons helicities. The fermion contribution is completely dominated by the top quark and interferes destructively with W-boson loop contribution. For opposite initial photon helicities, where the Higgs boson contribution is absent, the value of the cross section of Z_LZ_L pair production is about 1 fb or less (Fig. 2b). The dip near $\sqrt{s_{\gamma\gamma}} = 300$ GeV for fermion contribution in Fig. 2b is due to destructive interference between light fermion and top quark contributions. The most striking feature is the transversely polarized Z_TZ_T pair production cross section of the order of hundreds of femtobarns (see Fig. 2e-f), which does not decrease at high energies. It is completely dominated by the W loop contribution and for $m_H > 400$ GeV exceeds both Z_LZ_L and Z_LZ_T production cross sections.

Fig. 3 gives the angular distributions for Z_LZ_L, Z_LZ_T and Z_TZ_T pair production for equal and opposite incoming photon helicities at $\sqrt{s_{\gamma\gamma}} = 500$ GeV. We see that Z_TZ_T pair production cross section is peaking in forward or backward directions. Although the angular cut will enhance the Z_LZ_L contribution, nevertheless for any cut the transverse Z pair production cross section will be at least an order of magnitude larger than longitudinal Z pair production cross section.

The effect of large top quark mass is illustrated in Fig. 4. The most sensitive to m_t cross section of longitudinal Z pair production for equal initial photons helicities is shown for different Higgs boson masses of 300, 500, 800, 1000 GeV and infinitely heavy Higgs boson and top quark masses of 120 and 200 GeV. For Higgs boson masses heavier than 500 GeV and $m_t = 200$ GeV strong destructive interference between W and top quark contributions is observed. For infinitely heavy Higgs boson the cross section grows with energy at $\sqrt{s_{\gamma\gamma}} > 1$ TeV. Enhanced longitudinal Z_LZ_L pair production at high energies for heavy Higgs boson mass was estimated in [16] using the equivalence theorem. The complete SM calculation shown here gives reasonable agreement for the heavy Higgs case.

4.2. ZZ pair production at Photon Linear Collider

All e^+e^- colliders are also $\gamma\gamma$ colliders. However, the $\gamma\gamma$ luminosity resulting from the Weizsäcker-Williams spectrum of photons falls rapidly as a function of the $\gamma\gamma$ invariant mass

$$\frac{dL^{WW}_{\gamma\gamma}}{d\tau} = \frac{1}{\tau}\left(\frac{\alpha}{2\pi}\log\frac{s}{4m_e^2}\right)^2\left[(2+\tau)^2\log\frac{1}{\tau} - 2(1-\tau)(3+\tau)\right]. \qquad (4.2)$$

We show in Fig. 5 the total cross sections for ZZ pair production in e^+e^- collisions calculated using equivalent photon approximation (4.2) for different polarizations of Z-bosons and $m_H = 300$ and 500 GeV as a function of the e^+e^- c.m.s. energy. The main contribution comes from the transverse Z_TZ_T pair production having the cross section less than or about 1 fb at $\sqrt{s} < 1.5$ TeV. The main background to the observation of the reaction $\gamma\gamma \to ZZ$ in e^+e^- collisions will be the tree level SM process $e^+e^- \to ZZ\gamma$ with a much larger cross section. *E.g.*, at $\sqrt{s} = 500$ GeV this cross section is 14.7 fb with the following cuts imposed on photon transverse momentum: $p_T^\gamma > 20$ GeV and $\theta_{e\gamma} > 15^0$ [33]. Thus, the reaction $\gamma\gamma \to ZZ$ can hardly be observed in e^+e^- collisions.

By Compton backscattering of laser photons off the linac electron or positron beams, one can produce high luminosity $\gamma\gamma$ collisions with significantly harder $\gamma\gamma$ spectrum and a substantially higher luminosity at large $E_{\gamma\gamma}$ than Weizsäcker-Williams spectrum and luminosity [5–9]. In addition, a high degree of circular polarization for each of the colliding photons can be achieved by polarizing the incoming electron or positron beams and laser beams [6]. The cross section of the ZZ pair production in polarized $\gamma\gamma$ collisions is given by

$$d\sigma_{\lambda_3\lambda_4} = \int_{4m_Z^2/s}^{y_m^2} d\tau \frac{dL_{\gamma\gamma}}{d\tau}\left(\frac{1+\langle\xi_1\xi_2\rangle}{2} d\hat{\sigma}_{++\lambda_3\lambda_4}(\hat{s}) + \frac{1-\langle\xi_1\xi_2\rangle}{2} d\hat{\sigma}_{+-\lambda_3\lambda_4}(\hat{s})\right) \quad (4.3)$$

where

$$\frac{dL_{\gamma\gamma}}{d\tau} = \int_{\tau/y_m}^{y_m} \frac{dy}{y} f_\gamma(x,y) f_\gamma(x,\tau/y), \quad (4.4)$$

$$\tau = \hat{s}/s, \quad y = E_\gamma/E_b, \quad y_m = x/(x+1), \quad x \equiv 4E_b\omega_0/m_e^2.$$

Here E_b is the energy of the electron beam, ω_0 is the laser photon energy. The photon momentum distribution function $f_\gamma(x,y)$ and mean helicities of the two photon beams ξ_i are given by equations (4) and (17) of Ref. [6]. As usual, the dimensionless parameter x has been taken to be equal to 4.8 to avoid undesirable backgrounds. In the following we assume that 90% electron (positron) beam longitudinal polarization ($\lambda_{e1,2} = \pm 0.45$) and 100% laser beam circular polarization ($\lambda_{\gamma 1,2} = \pm 1$) are achievable.

In Fig. 6 we show the cross section of the ZZ pair production at the Photon Linear Collider as a function of the e^+e^- c.m.s. energy. To get an idea of an observable cross section, we restrict the Z-boson production angle, $|\cos\theta_Z| < \cos 30^o$. We show curves for $m_t = 120$ GeV and $m_H = 300$, 500, 800, 1000 GeV and infinitely heavy Higgs boson. We consider different polarizations of the initial electron (positron) and laser beams: $2\lambda_{e1,2}\lambda_{\gamma 1,2} = -0.9$, which gives the photon-photon energy spectrum peaking just below the highest allowed photon-photon energy (Fig. 6a,b), and unpolarized incoming electrons (positrons) and laser photons $\lambda_{e1,2} = \lambda_{\gamma 1,2} = 0$ which give the flat $\gamma\gamma$ spectrum (Fig. 6c). Relative polarizations $\lambda_{e1,2}$, $\lambda_{\gamma 1,2}$ in Figs. 6a,b are such that colliding photons are produced mainly with equal (opposite) mean helicities $\langle\xi_1\xi_2\rangle \sim \pm 1$, respectively. As for the case of monochromatic photon-photon collisions, at high energies the cross section is dominated by the transversely polarized Z_TZ_T pair production. Obviously, the Higgs signal is most clearly seen in polarized $\gamma\gamma$ collisions with $\langle\xi_1\xi_2\rangle \sim 1$, Fig. 6a. However, for $m_H > 300$ GeV taking into account the realistic photon spectrum

makes the background from transverse $Z_T Z_T$ pairs even more severe than for the monochromatic $\gamma\gamma$ spectrum.

Fig. 7 presents the invariant mass distribution of Z-boson pairs. The contributions for $Z_L Z_L$, $Z_L Z_T$ and $Z_T Z_T$ as well as their sum are shown separately for $m_H = 250$ and 300 GeV at $\sqrt{s_{e^+e^-}} = 400$ GeV, $m_H = 250$, 300 and 350 GeV at $\sqrt{s_{e^+e^-}} = 500$ GeV, and $m_H = 500$, 800 GeV and ∞ at $\sqrt{s_{e^+e^-}} = 1500$ GeV. Helicities of the incoming electron (positron) and laser photon beams $\lambda_{\gamma 1} = \lambda_{\gamma 2} = -1$ and $\lambda_{e1} = \lambda_{e2} = 0.45$, corresponding to Fig. 6a, were taken. Also, angular cut $|\cos\theta_Z| < \cos 30^0$ was imposed. While clear Higgs boson peaks are observable at $\sqrt{s_{e^+e^-}} = 400$ GeV for $m_H = 250$ and 300 GeV, to observe the Higgs signal for $m_H \geq 350$ GeV would be a problem, if isolation of the longitudinally polarized $Z_L Z_L$ pair production would not be possible. And at $\sqrt{s_{e^+e^-}} = 1500$ GeV the suppression of the background from transverse $Z_T Z_T$ pair production by almost two orders of magnitude is needed for the observation of the heavy Higgs boson signal.

In Fig. 8 we show the transverse momentum distribution at $\sqrt{s_{e^+e^-}} = 500$ and 1500 GeV for the same parameters as in Fig. 7. The Jacobian peaks in the $Z_L Z_L$ signal are clearly seen.

It is well known that it is impossible to isolate the ZZ final state in the four-jet mode because of the much larger $\gamma\gamma \to W^+W^-$ tree-level continuum background [22]. The W^+W^- background can be eliminated by searching for ZZ events in the e^+e^-X, $\mu^+\mu^-X$ and $q\bar{q}\nu\bar{\nu}$ modes. They constitute 41% of all ZZ events. To estimate the event rates we have taken $\mathcal{L}_{e^+e^-} = 10^{33}\text{cm}^{-2}\text{s}^{-1}$, implying

$$\int dt \mathcal{L}_{\gamma\gamma} = \int dt \mathcal{L}_{e^+e^-} = 10 \text{ fb}^{-1} \tag{4.5}$$

for a standard collider year, and multiplied the cross section (with the angular cut imposed) by the above branching ratio factor. For $m_H = 300$ GeV at $\sqrt{s_{e^+e^-}} = 400$ GeV and the invariant mass of ZZ pair in the interval $290 < M_{ZZ} < 310$ GeV 100 events per year would be observed. If we take ZZ pair production for $m_H = 250$ GeV, which has a smooth cross section in the interval considered, as a background, the number of background events (B) will be $B = 30$. The number of signal events (S) is then $S = 70$ and the number of standard deviations ($N_{SD} \equiv S/\sqrt{B}$) is greater than 10. But already for Higgs boson mass of 350 GeV at $\sqrt{s_{e^+e^-}} = 500$ GeV, where cross section for $m_H = 350$ GeV has a maximum, the situation is different. While the event rate for $m_H = 350$ GeV in the interval $325 < M_{ZZ} < 375$ GeV is 82, the number of background events, (*i.e.*, for $m_H = 250$ GeV), is $B = 61$,

and the number of standard deviations is less than 3. Thus, the conclusion of Ref. [15] that for $m_H > 2m_Z$ the ZZ mode can be used for all Higgs masses up to the $\gamma\gamma$ collider kinematic limit, which was based on the requirement of 5 signal events for detection, is not quite true.

On the other hand, the large cross section of the transverse $Z_T Z_T$ pair production in photon-photon collisions is purely one-loop prediction of the SM as a renormalizable nonabelian local gauge theory. Moreover, as it is shown in Fig. 2 at high energies the value of the cross section is dominated by the boson loops contributions and is sizable irrespective of the presence of a light Higgs boson peak. At $\sqrt{s_{e^+e^-}} = 500$ GeV and infinitely heavy Higgs boson about 200 (130) ZZ pairs yearly would be observed in W^+W^--background-free modes $ZZ \to e^+e^-X$, $\mu^+\mu^-X$, $q\bar{q}\nu\bar{\nu}$ in polarized (unpolarized) $\gamma\gamma$ collisions with angular cut and photon polarizations $\langle\xi_1\xi_2\rangle \sim 1$ ($\langle\xi_1\xi_2\rangle = 0$), corresponding to Fig. 6a (Fig. 6c). At $\sqrt{s_{e^+e^-}} = 1$ TeV 370 (340) ZZ pairs would be produced in polarized (unpolarized) photon-photon collisions. So, even assuming 50% experimental acceptance one can hope to detect a hundred ZZ pairs yearly at the Photon Linear Collider realized at the 500 GeV NLC.

In principle, ZZ pair production cross section in $\gamma\gamma$ collisions will be sensitive to the presence of the anomalous γWW, $\gamma\gamma WW$, ZWW and $ZZWW$ gauge-boson couplings. As a result of the gauge invariance the effects of non-renormalizable $SU(2) \times U(1)$ invariant dimension-6 effective operators [34] are logarithmically divergent non-standard deviations of the $\gamma\gamma \to ZZ$ helicity amplitudes. The influence of the anomalous couplings on the decay of the Higgs boson into two photons was studied in Refs. [35]. To estimate the effect of the non-standard vertices from other diagrams requires additional calculations. The QCD background to ZZ pair production is the resolved photon contribution via quark-antiquark and gluon-gluon fusion $q\bar{q} \to ZZ$, $gg \to ZZ$. As the quark (gluon) structure functions are peaking at small x and the corresponding parton cross sections decrease at high energies (because only quark exchanges contribute), the resolved photon contribution to ZZ pair production in $\gamma\gamma$ collisions is negligible. *E.g.*, the cross section of the sub-process $q\bar{q} \to ZZ$ lies in the range $0.2 \div 0.3$ fb at the photon-photon c.m.s. energy of $500 \div 1000$ GeV.

Moreover, the number of ZZ pair production events in photon-photon collisions is approximately the same as the number of the triple vector boson WWZ production events in e^+e^- collisions. The process $e^+e^- \to W^+W^-Z$ was proposed to study anomalous vector boson quartic couplings and its

improved Born SM cross section is 39.88 fb at 500 GeV [33]. If the W's are not reconstructed from their decays into τ's, this corresponds to 268 events assuming luminosity of 10 fb^{-1} and 100% efficiency [33].

4.3. ZZ pair production in Heavy-Ion Colliders

Another potential source of the high energy photon-photon collisions is heavy-ion collider. The ZZ pair would be produced in collateral collisions via $\gamma\gamma$ fusion, with two heavy ions remaining untouched. This would extremely reduce the QCD background, as it was first noted in the proposal to study the intermediate mass Higgs boson at heavy-ion collider [36]. The total cross section for ZZ pair production in ^{206}Pb ions collisions

$$^{206}Pb + {}^{206}Pb \to {}^{206}Pb + {}^{206}Pb + Z + Z \tag{4.6}$$

was calculated using the effective $\gamma\gamma$ luminosity obtained using the Weizsäcker-Williams approximation formulated in the impact-parameter space [37]. The resulting cross sections of $Z_L Z_L$, $Z_L Z_T$ and $Z_T Z_T$ pair production as a function of the energy per nucleon are shown in Fig. 9. Longitudinally polarized $Z_L Z_L$ pair production is shown for $m_H = 300$ and 500 GeV. The other curves are insensitive to the value of the Higgs boson mass. Energy $E \sim 8$ TeV/nucleon corresponds to the SSC, while $E \sim 3.2$ TeV/nucleon to the LHC. The cross section of the dominating transverse $Z_T Z_T$ pair production at the SSC heavy-ion collider would be two orders of magnitude larger than that at the Photon Linear Collider. However, with an expected luminosity of $10^{27} \div 10^{28}$ cm^{-2} s^{-1} at SSC one could produce one ZZ pair per year at most. It is, thus, unrealistic to observe ZZ pair production in photon fusion at heavy-ion collider.

5. Conclusions

We have studied the coupling of two photons with two Z-bosons via SM bosonic loops. Explicit formulae for all helicity amplitudes were obtained. We then applied these results to the production of Z-boson pairs at a future e^+e^- linear collider (with center of mass energy $E_{e^+e^-} = 500 \div 1000$ GeV) operating in a $\gamma\gamma$ collider mode. The cross section of transversely polarized $Z_T Z_T$ pair production is large (of the order of hundreds of femtobarns) and does not decrease with energy. It is dominated by the bosonic loop contribution, which

gives helicity amplitudes proportional to s in the limit $s \to \infty$ and finite $t(u)$. It would represent a severe irreducible background to the observation of the Higgs boson with $m_H > 350$ GeV if Z-boson polarization would not be detected. Also, enhanced longitudinal $Z_L Z_L$ pair production, predicted in different models, would have rates at least an order of magnitude smaller than transverse $Z_T Z_T$ pair production. Anyway, hundreds of Z-boson pairs yearly would be observed at Photon Linear Collider in the well reconstructable decay modes $ZZ \to e^+e^-X$, $\mu^+\mu^-X$, $q\bar{q}\nu\bar{\nu}$ irrespective of the value of the Higgs boson mass. Having the ability to achieve substantial polarization for the colliding photon beams will increase rates by a factor of two at e^+e^- center of mass energy of 500 GeV. Nonlinear interaction of two photons with two Z-bosons is a pure one-loop effect of the SM as renormalizable nonabelian local gauge theory. As such, it is sensitive to the presence of the anomalous triple and quartic gauge boson couplings which spoil subtle cancellations between different contributing diagrams at the one-loop level. Moreover, the event rates for Z-boson pair production in $\gamma\gamma$ collisions are approximately the same as for tree-level triple W^+W^-Z gauge boson production in e^+e^- collisions at NLC energies.

Finally, the potential of a Photon Linear Collider based on a back-scattered laser beam facility for detecting Z boson pairs is by far superior the possibilities for ZZ production via equivalent photon fusion in the reaction $e^+e^- \to e^+e^-ZZ$ or in heavy ion collisions $^{206}Pb + {}^{206}Pb \to {}^{206}Pb + {}^{206}Pb + Z + Z$.

Acknowledgements

I wish to thank J.J. van der Bij for sending the erratum to reference [24] and C. Zecher for providing the computer code of formulas [24]. I would also like to thank E.E. Boos, S.S. Gershtein and I.F. Ginzburg for discussions. This work was supported, in part, by a Soros Foundation Grant awarded by the American Physical Society.

Appendix A.

The scalar two-, three- and four-point functions $B(p^2)$, $C(p_i, p_j)$ and $D(p_i, p_j, p_k)$ are defined as [30]

$$B_0(p^2) = \frac{1}{i\pi^2}\int \frac{d^4q}{(q^2-m_W^2)\left((q+p)^2-m_W^2\right)}, \tag{A.1}$$

$$C(p_i,p_j) = \frac{1}{i\pi^2}\int \frac{d^4q}{(q^2-m_W^2)\left((q+p_i)^2-m_W^2\right)\left((q+p_i+p_j)^2-m_W^2\right)}, \tag{A.2}$$

$$D(p_i,p_j,p_k) = \frac{1}{i\pi^2}\int \frac{d^4q}{(q^2-m_W^2)\left((q+p_i)^2-m_W^2\right)\left((q+p_i+p_j)^2-m_W^2\right)\left((q+p_i+p_j+p_k)^2-m_W^2\right)}, \tag{A.3}$$

Notations used in the text are the following

$$\begin{aligned} B(p^2) &= B_0(p^2) - B_0(m_Z^2), \\ C_0(s) &= C(p_1,p_2), \quad C(s) = C(p_3,p_4), \\ C(t) &= C(p_2,p_3), \quad C(u) = C(p_1,p_3), \\ D(s,t) &= D(p_1,p_2,p_3), \quad D(s,u) = D(p_2,p_1,p_3), \\ D(t,u) &= D(p_1,p_3,p_2). \end{aligned} \tag{A.4}$$

Expressions for the vertex functions are given, *e.g.*, in Refs. [24, 38].

Auxiliary functions Q and Q_2 which are associated with a simple and double poles in Y are defined as

$$Q(s,t,u) = stD(s,t) - sC_0(s) + (t-u)C(s) - 2(t-m_Z^2)C(t); \tag{A.5}$$

$$\begin{aligned} Q_2(s,t,u) = {} & Y\Big\{2\frac{t}{s_4}\Big(4stC(t) + t(t-u-4s)C(s) - (t-u)B(s)\Big) \\ & -2tB(t) + 2m_W^2\Big(sC_0(s) + 2(t-m_Z^2)C(t) - (t-u)C(s)\Big)\Big\} \\ & +st^2\Big\{\Big(C(t)-C(s)\Big)\frac{(4t+s)^2}{2s_4} + \frac{4t-s}{2}C(t) + \frac{3s-4t}{2}C(s) \\ & +stD(s,t) - sC_0(s)\Big\}; \end{aligned} \tag{A.6}$$

These poles are artefacts of the tensor reduction algorithm [29] and functions Q and Q_2 should have simple and double zeroes, respectively, at $Y = 0$. In fact expressions (A.5,A.6) can be obtained considering reduction to a sum of scalar vertex functions of the following integrals

$$\int d^4q \frac{(q\cdot v)^2}{(q^2-m_W^2)\left((q+p_1)^2-m_W^2\right)\left((q+p_1+p_2)^2-m_W^2\right)\left((q+p_1+p_2+p_3)^2-m_W^2\right)}$$
$$\propto Y, \tag{A.7}$$
$$\int d^4q \frac{(q\cdot v)^4}{(q^2-m_W^2)\left((q+p_1)^2-m_W^2\right)\left((q+p_1+p_2)^2-m_W^2\right)\left((q+p_1+p_2+p_3)^2-m_W^2\right)}$$
$$\propto Y^2, \tag{A.8}$$

where compact definitions are introduced with the use of generalized Kronecker deltas

$$v_\mu = \delta^{p_1,p_2,\mu}_{p_1,p_2,p_3}, \quad \delta^{p_1,p_2,p_3}_{p_1,p_2,p_3} = sY/4. \tag{A.9}$$

Differentiating expressions (A.7,A.8) with respect to p_3 two and four times, respectively, it can be shown that combinations Q/Y and Q_2/Y^2 are finite as $Y \to 0$ and are given by

$$\frac{t}{Y}Q(s,t,u)\Big|_{Y=0} = \frac{2}{ss_4}\left((t-u)B(s)-(t^2-m_Z^4)C(s)\right)+\frac{2}{s}B(t)$$
$$-2m_W^2 D(s,t); \tag{A.10}$$
$$\frac{1}{Y^2}Q_2(s,t,u)\Big|_{Y=0} = \frac{1}{t}\Big(6m_W^4 D(s,t)+\frac{(t+6m_W^2)t_1^2}{s^2t}B(t)+\frac{t+m_Z^2}{2s_4}+\frac{t_1}{2s}$$
$$+\Big(\frac{3(1+4c_W^2)t_1}{4s}+\frac{(17-12c_W^2)t+3m_Z^2-12m_W^2}{4s_4}+\frac{3m_Z^2(t+m_Z^2)}{s_4^2}\Big)B(s)\Big)$$
$$+\frac{1}{4}\Big(\frac{(t+m_Z^2)((21-8c_W^2)t+9m_Z^2-8m_W^2)}{s_4^2}-\frac{(3+8c_W^2)t_1}{s}$$
$$-\frac{3m_Z^2-8m_W^2}{s_4}\Big)C(s). \tag{A.11}$$

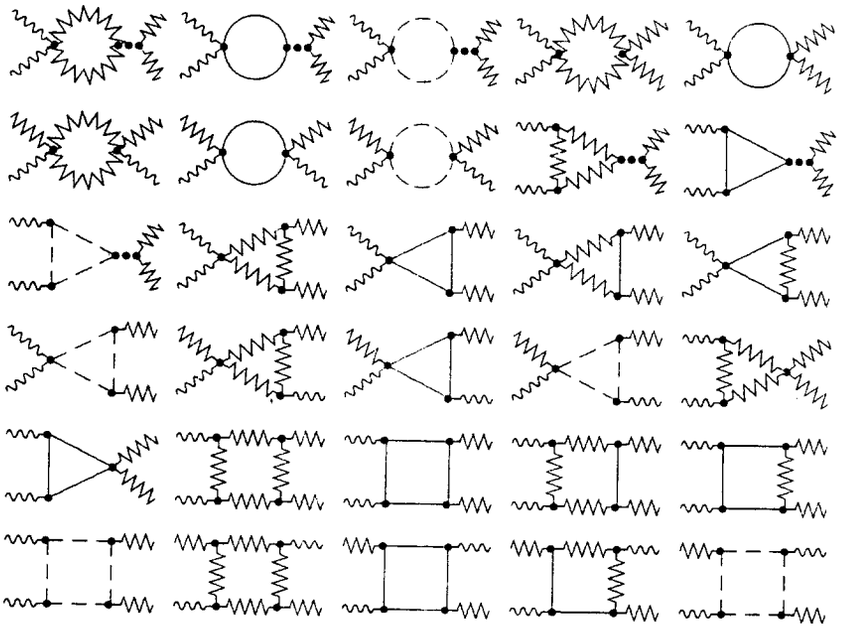

Fig. 1. Feynman graphs contributing to the process $\gamma\gamma \to ZZ$. Notations are the following: photon – wavy line, Higgs boson – dotted line, W, Z bosons – zigzag lines, charged NG scalar – solid line, FP ghost – dashed line.

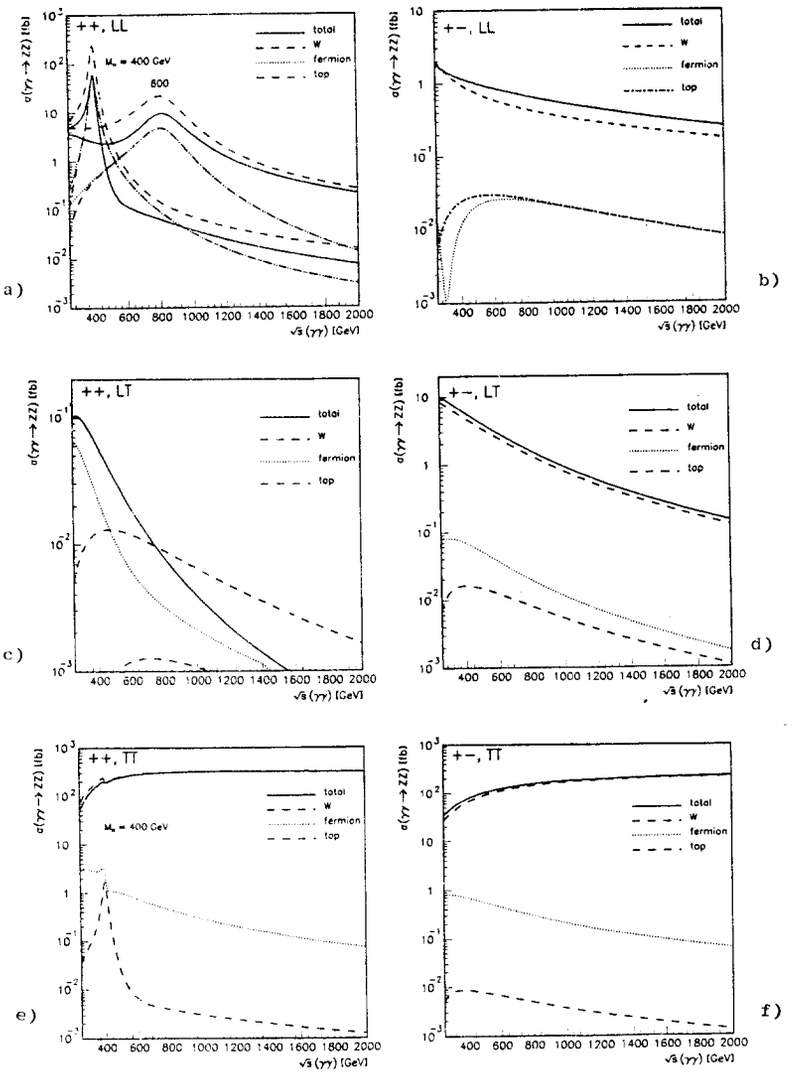

Fig. 2. Total cross section of ZZ pair production in monochromatic photon-photon collisions versus $\gamma\gamma$ c.m.s. energy for different helicities of the incoming photons and outgoing Z-bosons. Total cross sections (solid line) as well as boson loop contribution (dashed line), fermion loop contribution (dotted line) and top quark loop contribution (dot-dashed line) are shown. For equal photon helicities $\lambda_1 = \lambda_2 = 1$ Higgs boson mass was taken to be 400 and 800 GeV for longitudinal $Z_L Z_L$ pair production (Fig. 2a) and $m_H = 400$ GeV for transverse $Z_T Z_T$ pair production (Fig. 2e).

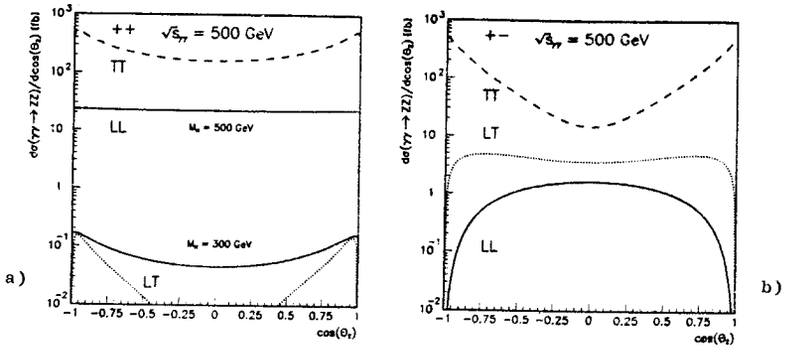

Fig. 3. Angular, $\cos(\theta_Z)$, distribution of Z-bosons produced in monochromatic photon-photon collisions at $\sqrt{s_{\gamma\gamma}} = 500$ GeV for equal $\lambda_1 = \lambda_2 = 1$ (Fig. 3a) and opposite $\lambda_1 = -\lambda_2 = 1$ (Fig 3b) photon helicities. Curves for $Z_L Z_L$ (solid line), $Z_T Z_T$ (dashed line) and $Z_L Z_T$ (dotted line) production are shown. For longitudinal $Z_L Z_L$ pair production and equal photon helicities curves for $m_H = 300$ and 500 GeV are shown. The effect of the variation of the Higgs mass on transverse $Z_T Z_T$ pair production cross section is negligible.

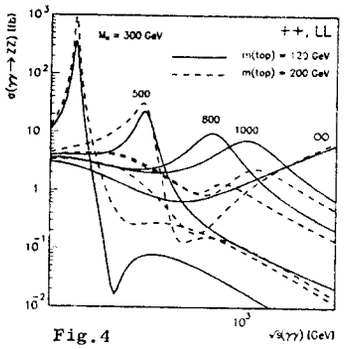

Fig.4

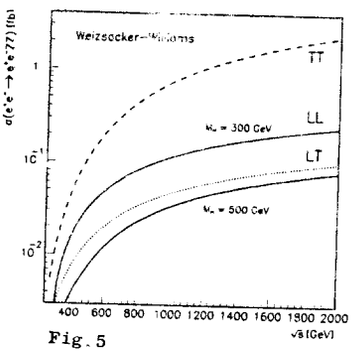

Fig. 5

Fig. 4. Total cross section of the longitudinal $Z_L Z_L$ pair production versus $\sqrt{s_{\gamma\gamma}}$ for Higgs boson masses of 300, 500, 800, 1000 GeV and infinity. To illustrate the variation with the top quark mass we show curves for $m_t = 120$ GeV (solid line) and $m_t = 200$ GeV (dashed line).

Fig. 5. Total cross section of the Z-boson pair production via $\gamma\gamma$ fusion in e^+e^- collisions computed in the Weizsäcker-Williams approximation. Notations are the same as in Fig. 3. Curves for $m_H = 300$ and 500 GeV are shown.

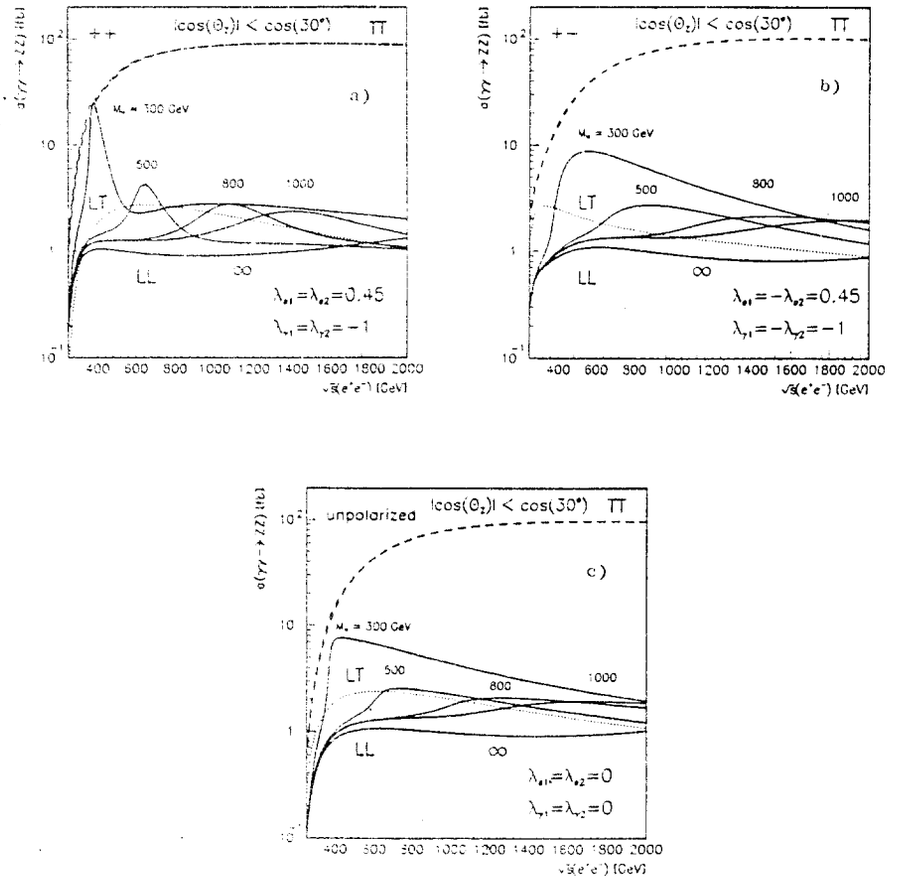

Fig. 6. Cross section of the ZZ pair production in $\gamma\gamma$ collisions versus c.m.s. energy of the e^+e^- collisions computed taking into account photon spectrum of the backscattered laser beams. Both Z-bosons have $|\cos\theta_Z| < \cos 30^0$. Curves for polarized initial electron and laser beams producing mainly high energy photons with equal helicities $\langle\xi_1\xi_2\rangle \sim 1$ (Fig. 6a) and opposite helicities $\langle\xi_1\xi_2\rangle \sim -1$ (Fig. 6b), as well as for unpolarized initial beams (Fig. 6c) are shown. Notations are the same as in Fig. 3. Different curves for longitudinal Z_LZ_L pair production correspond to Higgs boson masses of 300, 500, 800, 1000 GeV and infinity. Effect of the Higgs boson mass variation on transverse Z-boson pair production is negligible.

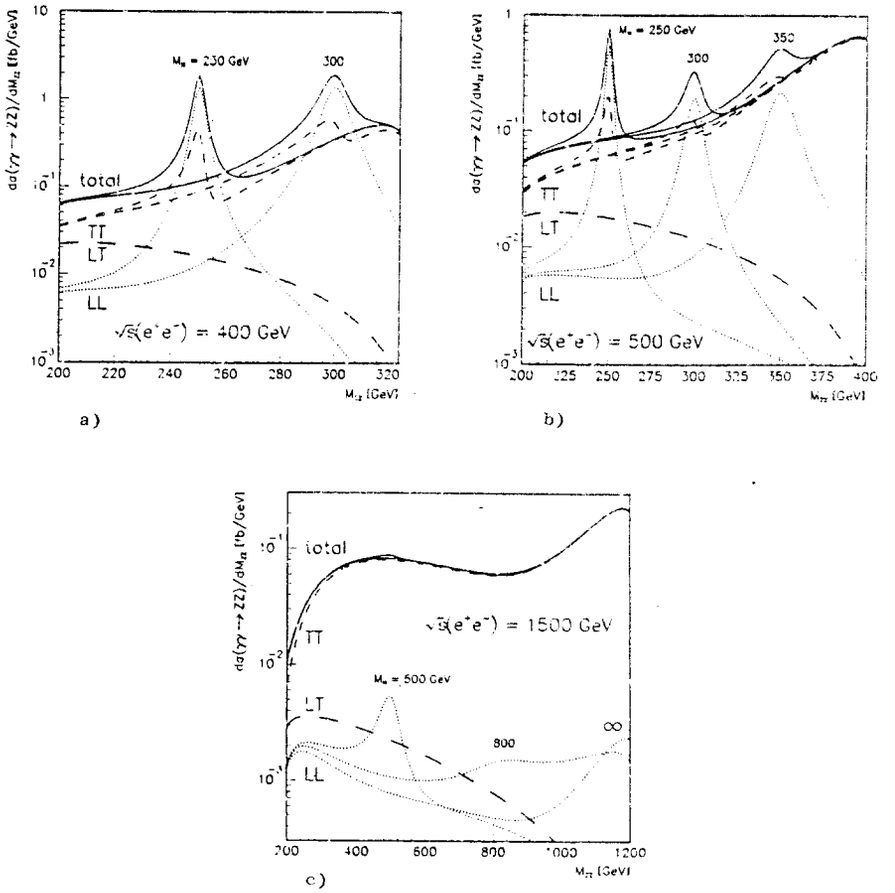

Fig. 7. The invariant mass, M_{ZZ}, distribution of Z-bosons for $\gamma\gamma \to ZZ$ in photon-photon collisions at (a) $\sqrt{s_{e^+e^-}} = 400$ GeV and $m_H = 250$ and 300 GeV, (b) $\sqrt{s_{e^+e^-}} = 500$ GeV and $m_H = 250$, 300 and 350 GeV and (c) $\sqrt{s_{e^+e^-}} = 1500$ GeV and $m_H = 500$, 800 GeV and infinity. Both Z-bosons have $|\cos\theta_Z| < \cos 30^0$. Polarizations of the electrons and laser beam photons $\lambda_{e1} = \lambda_{e2} = 0.45$, $\lambda_{\gamma 1} = \lambda_{\gamma 2} = -1$ were chosen, corresponding to high energy photons collisions with mainly equal helicities $\langle \xi_1 \xi_2 \rangle \sim 1$. Curves for $Z_L Z_L$ (dotted line), $Z_T Z_T$ (dashed line) and $Z_L Z_T$ (long dashed line) production are shown in addition to the sum over all polarizations of the Z-boson (solid line).

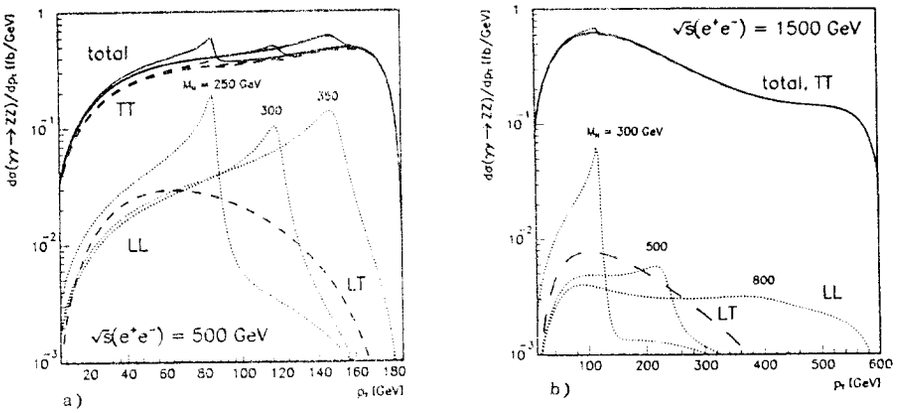

Fig. 8. The transverse momentum, p_{TZ}, distribution of Z-bosons for $\gamma\gamma \to ZZ$ in photon-photon collisions at (a) $\sqrt{s_{e^+e^-}} = 500$ GeV and $m_H = 250$, 300 and 350 GeV and (b) $\sqrt{s_{e^+e^-}} = 1500$ GeV and $m_H = 300$, 500 and 800 GeV. Notations are the same as in Fig. 7.

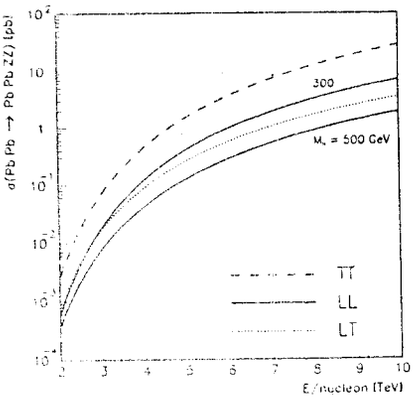

Fig. 9. Total cross section for $^{206}Pb + {}^{206}Pb \to {}^{206}Pb + {}^{206}Pb + Z + Z$ as a function of the energy per nucleon. LHC and SSC correspond to 3.2 and 8 TeV/nucleon, respectively. Curves for $m_H = 300$ and 500 GeV are shown.

References

[1] J.F. Gunion, H.E. Haber, G. Kane and S. Dawson, *The Higgs Hunter's Guide* (Addison-Wesley Publishing Company, Reading, MA, 1990).

[2] J.F. Gunion, UCD-92-20 (1992);
S. Dawson, BNL-47237 (1992);
Z. Kunszt, ETH-TH/92-20 (1992).

[3] V. Barger, K. Cheung, B.A. Kniehl and R.J.N. Phillips, MAD/PH/610 (1992).

[4] H.E. Haber, SCIPP 92/10 (1992); to appear in *Proceedings of the Workshop on Physics and Experiments with Linear Colliders*, Saariselkä, Finland, September 9-14, 1991.

[5] I.F. Ginzburg, G.L. Kotkin, V.G. Serbo and V.I. Telnov, Pis'ma ZhETF 34 (1981) 514; Nucl. Instr. Methods 205 (1983) 47.

[6] I.F. Ginzburg, G.L. Kotkin, S.L. Panfil, V.G. Serbo and V.I. Telnov, Nucl. Instr. Methods 219 (1984) 5.

[7] T.L. Barklow, SLAC-PUB-3564 (1990), to appear in *The Proceedings of the 1990 DPF Summer Study on High Energy Physics: Research Directions for the Decade*, Snowmass, CO, June 25-July 13, 1990.

[8] V.I. Telnov, to appear in *Proceedings of the Workshop on Physics and Experiments with Linear Colliders*, Saariselkä, Finland, September 9-14, 1991; Proceedings *Third International Workshop on Linear Colliders LC91*, Protvino, USSR, September 17-27, 1991.

[9] D.L. Borden, D.A. Bauer and D.O. Caldwell, preprint SLAC-PUB-5715, UCSB-HEP-92-01, 1992.

[10] R. Kleiss, Z. Kunszt and J. Stirling, Phys. Lett. B253 (1991) 269;
J.F. Gunion, Phys. Lett. B261 (1991) 510;
W. Marciano and F. Paige, Phys. Rev. Lett. 66 (1991) 2433.

[11] SDC Collaboration, Letter of Intent, SDC report, SDC-90-151 (1990) and the SDC Technical Design Report, SDC report, SDC-92-201 (April, 1992).

[12] L* Collaboration Letter of Intent, report SSCL-SR-1154 (1990);
EMPACT Collaboration Letter of Intent, report SSCL-SR-1155 (1990);
GEM Collaboration Letter of Intent, report SSCL-SR-1184.

[13] Contributions to *Proceedings of the Large Hadron Collider Workshop*, edited by G. Jarlskog and D. Rein, Aachen (1990), CERN 90-10, ECFA 90-133, Vol. II.

[14] ASCOT, EAGLE, CMS, and L* Collaborations, Expressions of Interest, presented at *General Meeting on LHC Physics and Detectors Towards the LHC Experimental Program*, Evian-les-Bains, France (1992).

[15] J.F. Gunion and H.E. Haber, UCD-92-22 (1992).

[16] E.E. Boos, G.V. Jikia, Phys. Lett. B275 (1992) 164.

[17] M.E. Peskin, Workshop on Physics and Experiments with Linear Colliders, Saariselkä, Finland, September 9-14, 1991; preprint SLAC-PUB-5798, 1992.

[18] M. Herrero and E. Ruiz-Morales, FTUAM92/22 (1992).

[19] M.S. Chanowitz, Proc. of the 2-nd KEK Topical Conference on e^+e^- Collision Physics, Tsukuba, Japan, November 26-29, 1991; Phys. Rev. Lett. 69 (1992) 2037.

[20] I.F. Ginzburg, preprint INP Novosibirsk 28(182) (1990).

[21] G. Bélanger and F. Boudjema, Phys. Lett. B288 (1992) 210.

[22] I.F. Ginzburg, G.L. Kotkin, S.L. Panfil and V.G. Serbo, Nucl. Phys. B228 (1983) 285;
E. Yehudai, Phys. Rev. D44 (1991) 3434.

[23] D.A. Dicus, C. Kao, and W.W. Repko, Phys. Rev. D36 (1987) 1570;
D.A. Dicus, Phys. Rev. D38 (1988) 394.

[24] E.W.N. Glover, J.J. van der Bij, Nucl. Phys. B321 (1989) 561; preprint CERN-TH.5248/88, Erratum.

[25] G.V. Jikia, Phys. Lett. B298 (1993) 224.

[26] A.I. Vainstein, M.B. Voloshin, V.I. Zakharov and M.A. Shifman, Yad. Fiz. 30 (1979) 1368.

[27] R. Karplus and M. Neuman, Phys. Rev. 80 (1950) 380; Phys. Rev. 83 (1951) 776.

[28] V. Costantini, B. De Tollis, and G. Pistoni, Nuovo Cimento A2 (1971) 733.

[29] G.J. van Oldenborgh and J.A.M. Vermaseren, Z. Phys. C - Part. and Fields 46 (1990) 425.

[30] G. 't Hooft and M. Veltman, Nucl. Phys. B153 (1979) 365.

[31] J.A.M. Vermaseren, Symbolic Manipulation with FORM, published by CAN, Kruislaan 413, 1098 SJ Amsterdam, 1991, ISBN 90-74116-01-9.

[32] V.G. Gorshkov, Uspekhi Fiz. Nauk 110 (1973) 45.

[33] G. Bélanger and F. Boudjema, Phys. Lett. B288 (1992) 201.

[34] A. de Rújula et. al., Phys. Lett. B245 (1990) 640; Nucl. Phys. B357 (1991) 357; Nucl. Phys. B384 (1992) 3
A. de Rújula, in *The Proceedings of the 2-nd KEK Topical Conference on e^+e^- Collision Physics*, Tsukuba, Japan, November 26-29, 1991.

[35] H. König, Phys. Rev. D45 (1992) 1575;
M.A. Pérez and J.J. Toscano, Phys. Lett. B289 (1992) 381.

[36] E. Papageorgiu, Phys. Rev. D40 (1989) 92; Nucl. Phys. A498 (1989) 593.

[37] R.N. Cahn and J.D. Jackson, Phys. Rev. D42 (1990) 3690.

[38] G.V. Jikia, preprint IHEP 92-91, Protvino, 1992, submitted to Nucl. Phys. B.

Received 11 March, 1993

Г.Джикия

Рождение пар Z-бозонов в фотонном слиянии
на высокоэнергичном фотонном коллайдере.

Редактор А.А.Антипова. Технический редактор Л.П.Тимкина.

Подписано к печати II. 03. 93. Формат 60x90/I6.
Офсетная печать. Печ.л. 2,00. Уч.-изд.л. 2,23. Тираж 270.
Заказ 709. Индекс 3649. Цена II8 руб.

Институт физики высоких энергий, I42284, Протвино
Московской обл.

Индекс 3649

118 руб.

ПРЕПРИНТ 93-37, ИФВЭ, 1993